Intermetallics. Vol. 16. Núm. 3. 2008. Pag. 470-478
http://dx.doi.org/10.1016/j.intermet.2007.12.011

An equivalent time approach for scaling the mechanical alloying processes

J. J. Ipus[1], J. S. Blázquez[1], V. Franco[1], M. Millán[1], A. Conde[1], D. Oleszak[2], T. Kulik[2]

[1] Dpto. Física de la Materia Condensada, ICMSE-CSIC, Universidad de Sevilla, P.O. Box 1065, 41080, Sevilla, Spain.

[2] Faculty of Materials Science and Engineering, Warsaw University of Technology, ul. Woloska 141, 02-507, Warsaw, Poland.

ABSTRACT. Dynamics of a single ball into a planetary ball mill is analyzed leading to a cubic dependence of the power transferred during milling with the rotational speed, Ω. This leads to the definition of an equivalent time to describe the state of ball milled powders independently of Ω. Mechanical alloying of $Fe_{75}Ge_{20}Nb_5$ composition is studied by a combination of experimental techniques (differential scanning calorimetry, scanning electron microscopy, energy dispersive x-ray spectrometry, x-ray diffraction, Mössbauer spectrometry and vibrating sample magnetometry) and results evidence a good agreement with the predictions of the equivalent time approach.

Keywords: C. Mechanical alloying and milling; C. Nanocrystals

Corresponding author: Prof. A. Conde
Departamento de Física de la Materia Condensada. Universidad de Sevilla.
Apartado 1065, 41080 Sevilla (Spain).
Phone: (34) 95 455 28 85
Fax: (34) 95 461 20 97
E-mail: conde@us.es

Intermetallics. Vol. 16. Núm. 3. 2008. Pag. 470-478
http://dx.doi.org/10.1016/j.intermet.2007.12.011

1. Introduction

Ball milling has been shown as a very versatile technique for production of metastable systems: nanocrystalline, amorphous, supersaturated solid solutions, quasicrystals, etc [1]. Unlike ultra fast cooling techniques, which can freeze high temperature microstructures at low temperatures in a narrow compositional range around the eutectic, ball milling is applied to a wider compositional range. Mechanical evolution induced by ball milling is due to the energy transferred from the milling media to the powder particles, continuously submitted to fracture and cold welding processes which will define their final morphology. Among the different types of ball mills available, planetary ball mills are widely used to produce such metastable materials.

In order to understand the dynamics of planetary ball mills, several authors have used the approach of single ball dynamics and have extrapolated their results to actual milling processes using several balls [2,3,4,5,6,7,8]. These studies analyze the energy transferred per collision between the ball and the vial wall and the dependence of the ball trajectory on different parameters such as ratio between the frequencies of main disk and vials, ball to powder mass ratio and others [1,2,3,4,5,6,7,8,9,10]. Those results yield a parabolic dependence of the intensity of a single ball-powder interaction with the rotational speed. Moreover, the trajectory described by this single ball was found independent of the rotational speed [2]. These two features, as it will be shown in the following section of this paper, might lead to a cubic law for the estimated power transferred to the powder under a single ball approach. The reliability of this prediction is tested in the third section of the paper by studying the evolution of a mechanically alloyed $Fe_{75}Nb_5Ge_{20}$ powder at different milling intensities during different times.

Intermetallics. Vol. 16. Núm. 3. 2008. Pag. 470-478
http://dx.doi.org/10.1016/j.intermet.2007.12.011

2. Approach to the dynamics of the planetary ball mill

2.1 Movement of a single ball into the vial

Single ball approximation has been used in the literature to predict the energy transfer to powder during milling. In this section, a brief description of the rotational speed dependence of both the energy involved in different ball-powder interactions and the frequency of these events is given. Figure 1 shows a scheme of the planetary ball mill, where $\vec{R}$ is the position of the vial center and its modulus the radius of the main disk; $\vec{r}$, the position of the ball respect to the center of the vial, which modulus is the radius of the vial minus that of the ball; $\vec{p} = \vec{R} + \vec{r}$ is the position of the center of the ball; $\theta = \Omega t + \theta_0$ is the angle rotated by the main disk at time t and Ω its angular speed; $\alpha = \omega t + \alpha_0$ is the angle rotated by the vial at time t and ω its angular speed. In this scheme, the rotations of the vial and that of the main disk are opposite. Three orthogonal reference systems have been defined to position the ball at point P; a Cartesian inertial system $\left(\vec{i}, \vec{j}, \vec{k}\right)$ and two polar and non-inertial systems: $\left(\vec{e}_R, \vec{e}_\theta, \frac{\vec{\Omega}}{|\vec{\Omega}|}\right)$, which follows the rotation of the main disk, and $\left(\vec{u}_r, \vec{u}_\alpha, \frac{\vec{\omega}}{|\vec{\omega}|}\right)$, which follows the rotation of the vial.

In the simplified studied system, the particle movement must fulfill some requirements, also considered by other authors [3,4]:

- Only the movement of one ball is considered.
- The movement occurs in a plane.

Intermetallics. Vol. 16. Núm. 3. 2008. Pag. 470-478
http://dx.doi.org/10.1016/j.intermet.2007.12.011

- Only two forces are considered; the normal reaction of the vial wall over the ball, $\vec{N}$, and the friction force, $\vec{F}_\mu$.
- The particle keeps fixed at a point of the vial wall since $N>0$.
- When $N=0$, the ball detaches from the vial wall and moves freely until it impacts again with the vial wall.
- After the collision, the ball moves again stuck to the wall.

After analyzing the dynamics of the system and considering only the force component parallel to $\vec{u}_r$ an expression for N per mass unit of ball is found,

$$N/m = \omega^2 r + \Omega^2 R\cos(\theta+\alpha) \quad (1)$$

This expression is meaningful only for $N>0$, if $N=0$ the ball will detach from the vial wall, thus a detachment time, t_d, can be obtained as:

$$t_d = \frac{1}{\omega+\Omega}\left[\arccos\left(\frac{-\omega^2 r}{\Omega^2 R}\right)-(\alpha_0+\theta_0)\right] \quad (2)$$

Analogously to expression (1), considering the component parallel to $\vec{u}_\alpha$, an expression for F_μ per mass unit of ball is obtained,

$$F_\mu/m = \Omega^2 R\sin(\theta+\alpha) \quad (3)$$

This solution will apply if the ball is assumed to be fixed at a point of the vial wall. Once the ball detaches from the vial wall it moves freely with constant velocity until it collides again with the vial wall. In order to calculate the time of flight, t_f, the separation distance between the ball and the vial wall has been analyzed. In fact, the ball will

Intermetallics. Vol. 16. Núm. 3. 2008. Pag. 470-478
http://dx.doi.org/10.1016/j.intermet.2007.12.011

collide when $\left|\vec{R}-\vec{p}\right|$ equals the radius of the vial, r. Figure 2 shows the curve of the difference between the square of $\left|\vec{R}-\vec{p}\right|$ and the square radius of the vial as a function of time from the detachment for the planetary mill used in section 3, with R=0.125 m, r=0.017 m (it has been considered that the ball has a radius of 0.005 m), at Ω=150, 250 and 350 rpm, being the values of t_d and t_f of the same order of magnitude. By using different values of Ω, keeping constant the ratio ω/Ω, it can be observed that both t_d and t_f are proportional to 1/Ω (see expression (2) and inset of figure 2, respectively) and, therefore, the number of detachment and collision events remains constant along a period of rotation of the main disk.

For $t>t_d$, N=0 (as well as F_μ) and the ball is not in contact with the vial wall. After the ball collides with the wall, N will recover a non zero value. The trajectory of the ball, for both inertial and non-inertial reference systems are shown in figure 3. It can be observed that the point of collision, P_C, is different to the position of the detachment point at the time of collision, P_D'. Therefore, a phase angle, δ, must be included in the argument of the cosine function of equation (1). After the collision, the process is repeated continuously and figure 4 shows the value of N, solid line, during a rotational period of the main disk along with the analytical solution of equation (1), dotted line, for comparison.

2.2 Estimation of the dependence of the energy transfer on the frequency

The simple model described above can be used to propose a dependency of the energy transferred during milling from the balls and vial to the powder. Several

Intermetallics. Vol. 16. Núm. 3. 2008. Pag. 470-478
http://dx.doi.org/10.1016/j.intermet.2007.12.011

mechanisms can be considered as candidates for energy transfer from the balls and vial to the powder.

First, while the ball is in contact with the vial wall, the powder which is in between is compressed and sheared and the work done over the powder during this compression could be approximated to:

$$W_N = \int N\,dx \approx <N> d = k_1 \Omega^2 \tag{4}$$

where d is a distance of the order of the powder particle size (micrometer) and k_1 is a constant. For Ω=150 rpm, the energy transferred by unit mass of ball can be estimated as ~10^{-4} J/kg for d~1 μm. Analogously, it could be possible to estimate a similar order of magnitude for the shear work done by the friction force.

On the other hand, when the ball, after being detached, impacts against the vial wall, a change in its velocity is necessary to allow the ball to move with the vial again. This change implies a reduction in the kinetic energy of the ball, which can be calculated as:

$$\Delta E_C = \frac{1}{2} m\left(v(t_d)^2 - v_{imp}{}^2\right) \tag{5}$$

where $v(t_d)$ is the speed of the ball at the detachment time and v_{imp} is the modulus of the speed of the vial wall at P_C:

$$v(t_d) = \Omega R \sqrt{\left[\sin\left(\Omega t_d + \omega t_d\right)\right]^2 + \left[\cos\left(\Omega t_d + \omega t_d\right) + \frac{\omega r}{\Omega R}\right]^2} \tag{6}$$

$$v_{imp} = \Omega R \sqrt{\left[\sin\left(\Omega\left(t_d + t_f\right) + \omega\left(t_d + t_f\right) + \delta\right)\right]^2 + \left[\cos\left(\Omega\left(t_d + t_f\right) + \omega\left(t_d + t_f\right) + \delta\right) + \frac{\omega r}{\Omega R}\right]^2} \tag{7}$$

The values of ΔE_C per unit mass of ball, as it occurs for the estimated work of compression, and as expected by expressions (6) and (7), follows a Ω^2 law. For Ω=150 rpm the order of magnitude of the transferred energy is 1 J/kg per collision event.

Intermetallics. Vol. 16. Núm. 3. 2008. Pag. 470-478
http://dx.doi.org/10.1016/j.intermet.2007.12.011

Some authors have estimated the energy transferred to the powder, assuming a Hertzian collision approximation and after estimating the amount of powder in between the ball and the vial wall [4,6,8]. Several parameters affect the final results, as ball to powder mass ratio and elastic properties of the milling media as well as of the powder, etc, which were constant along the experiments performed in this work. Therefore, the Ω dependence of the energy transferred during the milling process is preserved.

As it has been shown in figure 4, during a period of rotation of the main disk, a constant number of compression events and impacts occur. Assuming the work done during each compression is described by equation (4) and that of each impact is described by equation (5), the average power could be estimated, for long times, as the whole work done during a period of rotation of the main disk divided by this time:

$$P = \frac{n\left(W_N + \Delta E_C\right)}{T} = k_2 \Omega^3 \tag{8}$$

where n is the constant number of events per period and k_2 is a constant. Therefore, the energy transferred after a time t would be proportional to Ω^3 and, if several values of Ω are used (keeping constant the ratio ω/Ω) an equivalent time, t_{eq}, can be defined as:

$$t_{eq} = t\left(\Omega / \Omega_0\right)^3 \tag{9}$$

where Ω_0 is a reference frequency (in the following study Ω_0=150 rpm, which is the lowest frequency used).

As milling time increases, energy is transferred from milling media to powder yielding microstructure evolution and different transformations [1]. Quantifying experimentally this energy is a difficult task as its acquisition is not completely reversible. In order to overcome these obstacles, some authors have proposed energy maps to approximately compare microstructures obtained from different milling conditions [3,8]. In this work, it has been assumed that the state of the powder is

Intermetallics. Vol. 16. Núm. 3. 2008. Pag. 470-478
http://dx.doi.org/10.1016/j.intermet.2007.12.011

univocally determined by the amount of energy transferred to the powders. Therefore, powder of $Fe_{75}Nb_5Ge_{20}$ composition has been characterized by using different structural and magnetic techniques after milling at different frequencies during different times, keeping constant the ω/Ω ratio. Results from different experimental techniques have been rescaled using an equivalent time defined by equation (9) with Ω_0=150 rpm.

3. Application to experimental results

3.1 Experimental techniques

$Fe_{75}Nb_5Ge_{20}$ composition was produced from pure powders (purity≥99 %) by ball milling in a Fritsch Pulverisette 5 planetary ball mill using hardened steel balls (10 mm diameter) and vials. The initial powder mass was 5 g and the ball to powder ratio 10:1. The ratio between the rotational speed of the vial (ω) and that of the main disk (Ω) was fixed to ω/Ω=-2. Three different values of Ω were used: 150, 250 and 350 rpm. Some powder was taken out after selected times (from 1 h to 150 h), opening and closing the vials in argon atmosphere to avoid oxygen and humidity contamination.

Size and morphology of the powder particles were studied by scanning electron microscopy (SEM) in a Jeol JSM-6460 LV and energy dispersive X-ray (EDX) analyses were performed using an Incax-sight of Oxford Instruments. The crystalline structure was studied by X-ray diffraction (XRD) using Cu-Kα radiation in a Bruker D8I diffractometer and the local environment of Fe atoms was analyzed by Mössbauer spectrometry (MS). Mössbauer spectra were recorded at room temperature in a transmission geometry using a ^{57}Co(Rh) source. The values of the hyperfine parameters were obtained by fitting with NORMOS program [11]. Thermal stability of the samples was studied by differential scanning calorimetry (DSC) using a Perkin-Elmer DSC7

Intermetallics. Vol. 16. Núm. 3. 2008. Pag. 470-478
http://dx.doi.org/10.1016/j.intermet.2007.12.011

under argon flow. Specific saturation magnetization, σ_S was measured in a Lakeshore 7407 vibrating sample magnetometer (VSM), applying a maximum field of 1.5 T.

3.2 Calorimetry

Figure 5 shows the DSC scans of the alloy after milling 150 h at different rotational speeds. Both samples milled at 250 and 350 rpm exhibit similar curves, showing a broad exothermic maximum generally ascribed to relaxation and crystal growth effects [1]. This fact implies that the energy released after heat treatment is not proportional to the amount of energy supplied by the milling media, as milling at 350 rpm must be more energetic than milling at 250 rpm. On the other hand, the sample milled at 150 rpm exhibits, along with the broad exotherm, an endothermic peak. This endotherm is ascribed to heterogeneities observed in the powder; as it will be shown later by XRD and MS techniques, several crystalline phases coexist in the powder formed after 150 h milling at 150 rpm. A detailed discussion on the thermal evolution of milled samples as a function of the milling time will be reported elsewhere [12] as it is out of the scope of the present paper.

3.3 Powder particle size and composition

SEM images were used to measure the average powder particle size, $<d>$, (statistic over an average of 200 particles per sample) as a function of time and rotational speed. Figure 6.a shows the values of $<d>$ as a function of time (upper panel) and the equivalent time defined by equation (9) (lower panel). For samples milled at 150 rpm, powder particle size keeps almost constant (~15 μm) for low milling times to decrease for longer times down to a constant value of ~5 μm. For samples milled at 250 rpm, <d> starts decreasing at very low milling times and the same constant value, ~5

μm, is observed for long milling times. For samples milled at 350 rpm, an almost constant value of ~10 μm is observed since very low milling times. The larger powder particle size in the alloy milled at 350 rpm could be linked to a higher temperature inside the vial during milling process, as the sequence of milling and pause intervals is the same independently of the rotational speed. In fact, for the same composition at milling intervals of 50 h, a powder particle size of ~22 μm [13], clearly larger than those reported here, is obtained after 150 h.

Using an EDX analyzer it was possible to measure the amount of Ge, Nb and Fe in the particles. A set of 20 spectra on different powder particles were obtained and the average concentration of these elements were around the nominal values. In addition, the Cr content due to contamination from the vials and balls was also measured. The Cr concentration is plotted in figure 6.b versus both the actual milling time and the equivalent one. For 350 rpm milled samples, it was possible to detect an increase of the amount of Cr content with the milling time. For 150 and 250 rpm, Cr contamination is negligible up to 150 h. Once the equivalent time is considered, a common behavior is observed, independently of the frequency used. Along with this Cr increase, a Fe contamination is expected but lower than the resolution of our equipment [14].

3.4 X-ray diffraction

Figure 7 shows the XRD patterns of samples milled at different frequencies during different milling times. These patterns can be classified into three different types: a) patterns in which the diffraction maxima of Nb are detectable; b) patterns in which a new intermetallic crystalline phase appears, with a peak at $2\theta \sim 37^{o}$; and c) patterns in which only a α-Fe(GeNb) bcc solid solution is detected. Table 1 shows the limits between the ranges at which the different types of XRD patterns are observed as a

function of both actual and equivalent times. The evolution of the XRD patterns can be generally described as follows: as milling time increases, Ge and Nb maxima decrease and disappear (t_{eq}<100 h), whereas a new phase is formed with a peak at 2θ~37º (t_{eq}>20 h). Further increase of the milling time yields the destruction of this phase (t_{eq}<100-150 h) and only a crystalline bcc solid solution is observed (t_{eq}>100-150 h). In order to analyze the evolution of the XRD patterns, the 2θ position and the full width at half maximum of the (110) peak of the bcc α-Fe(Ge,Nb) phase has been studied as a function of milling time and results are plotted in figures 8.a and b, respectively, as a function of the actual and equivalent times. Once the equivalent time is considered, a common evolution can be observed: for short milling times (t_{eq}<100 h), $2\theta_{(110)}$~44.8º, which corresponds to a lattice parameter *a*=2.86 Å, in agreement with pure α-Fe phase; whereas, for t_{eq}>150 h, $2\theta_{(110)}$ strongly decreases down to 44.2º, implying an increase of *a*=2.90 Å ascribed to the enrichment of the bcc α-Fe type phase in Ge and Nb, which are incorporated in the final bcc solid solution. Finally, for t_{eq}>400 h, $2\theta_{(110)}$ shifts to higher values again, which can be ascribed to the effect of contamination by Fe and Cr in agreement with figure 6.b. Figure 8.c shows the evolution of the area fraction of the bcc Fe and fcc Ge phases versus both the actual and equivalent milling times. Plots represented as a function of the defined equivalent time are independent of the milling intensity used.

3.5 Mössbauer spectrometry

Mössbauer spectra of samples milled for different times at different Ω are shown in figure 9. Depending on the spectra, three different types of fitting were done: a) using a single site with hyperfine magnetic field *HF*=33 T; b) using a site at *HF*=33 T plus one or two magnetic hyperfine field distributions (for low and high fields, respectively);

and c) using a single magnetic hyperfine field distribution. Table 2 shows the limits between the ranges at which the different types of Mössbauer fittings were performed as a function of both actual and equivalent times. As it occurs for XRD patterns, a general evolution can be described taking into account the equivalent time: for short milling times (t_{eq}<10-20 h), the local environment of Fe is that of bcc Fe and the presence of impurities or interface effects is negligible; but in the equivalent time range from 10-20 h to 100-150 h, the presence of impurities and interface effects yields the existence of Fe local neighborhoods different to that of pure α-Fe, whose contributions continuously increase, whereas that at 33 T decreases. Finally, for t_{eq}>100-150 h, there is no necessity of using a site contribution at 33 T and the MS spectra can be fitted with a single hyperfine field distribution.

As a tool to follow the progressive transformation, the evolution of the average hyperfine magnetic field, <*HF*>, has been studied as a function of the actual and the equivalent times and is shown in figure 10.a. As it occurred for previous studied magnitudes, the representation versus equivalent time yields a common behavior in agreement with the proposed Ω^3 dependence of the energy transferred during the milling process. The progressive reduction of <*HF*> is ascribed to Fe in Nb or Ge rich regions (low field contributions) or to Fe with a Fe rich neighborhood but different to that of pure α-Fe (high field contributions but lower than 33 T due to impurities or interface effects). Finally, at long milling times, an increase is observed, which could be related to the enrichment in Fe due to contamination as described above.

3.6 Specific saturation magnetization

Specific saturation magnetization of as-milled powder, σ_S, is shown as a function of actual time and equivalent time in figure 10.b. The evolution of σ_S as a

Intermetallics. Vol. 16. Núm. 3. 2008. Pag. 470-478
http://dx.doi.org/10.1016/j.intermet.2007.12.011

function of t_{eq} is independent of the frequency used and in agreement with the evolution of $<HF>$ described above. For short milling times, σ_S decreases down to a minimum value of about $1.6 \cdot 10^{-4}$ Tm^3kg^{-1}. However, at very long milling times (t_{eq}>1000 h), σ_S increases due to contamination.

Conclusions

A simple model based on the dynamics of a single ball into a planetary ball mill has been described. The model leads to a cubic dependence of the power transferred to the powder with the rotational speed of the main disk, assuming that the ratio between the angular speeds of the vial and the main disk are constant. This yields the definition of an equivalent time $t_{eq}=t\,(\Omega/\Omega_0)^3$.

Results of the model have been applied to powder particle size, contamination, microstructure and magnetic properties evolution of a $Fe_{75}Ge_{20}Nb_5$ alloy obtained by ball milling from pure powders. A fairly good overlapping of the experimental results for different milling intensities can be obtained after representing their evolution versus the equivalent time. It is worth mentioning that very different properties rescale according to this equivalent time, e. g. Cr contamination and microstructure evolution. An exception is observed for the powder particle size, which could be affected by the temperature achieved into the vial.

Acknowledgements

This work was supported by the Spanish Government and EU FEDER (Project MAT 2004-04618) and by the PAI of the Regional Government of Andalucía (Project P06-FQM-01823). J.J.I. acknowledges a fellowship from the Spanish Ministry of Education. J.S.B. acknowledges a research contract from the Regional Government.

Intermetallics. Vol. 16. Núm. 3. 2008. Pag. 470-478
http://dx.doi.org/10.1016/j.intermet.2007.12.011

References

[1] C. Suryanarayana, Prog. Mater. Sci. 46 (2001) 1-184.

[2] P. LeBrun, L. Froten, A. L. Delaey, Mater. Sci. Eng. A 161 (1993) 75-82.

[3] M. Abdellaui, E. Gaffet, Acta Metall. Mater. 43 (1995) 1087-1098.

[4] P. P. Chattopadhyay, I. Manna, S. Talapatra, S. K. Pabi, Mater. Chem. Phys. 68 (2001) 85-94.

[5] R. Hamzaoui, O Elkedim, E. Gaffet, J. Mater. Sci. 39 (2004) 5139-5142.

[6] T. H. Courtney, Mater. Trans. JIM 36 (1995) 110-122.

[7] F. Delogu, G. Cocco, J. Mater. Synth. Proc. 8 (2000) 271-277.

[8] M. Magini, A. Iasonna, Mater. Trans. JIM 36 (1995) 123-133.

[9] J. Eckert, L. Schultz, E. Hellstern, K. Urban, J. Appl. Phys. 64 (1988) 3224-3228.

[10] C. C. Koch, Mater. Trans. JIM 36 (1995) 85-95.

[11] R.A. Brand, J. Lauer, D.M. Herlach, J. Phys. F. Met. Phys. 13 (1983) 675-683.

[12] J. S. Blázquez, J. J. Ipus, M. Millán, V. Franco, A. Conde, D. Oleszak, T. Kulik, in preparation.

[13] J. S. Blázquez, V. Franco, C. F. Conde, A. Conde, Intermetallics 15 (2007) 1351-1360.

[14] F. Q. Guo, K. Lu, Nanostruct. Mater. 7 (1996) 509-517.

Intermetallics. Vol. 16. Núm. 3. 2008. Pag. 470-478
http://dx.doi.org/10.1016/j.intermet.2007.12.011

Table 1

Milling time ranges for the three types of XRD patterns: a) presence of bcc Nb maxima, b) presence of intermetallic phase and c) formation of a bcc solid solution

Ω (rpm)	$[\Omega/\Omega_0]^3$	a) bcc Nb		b) Intermetallic		c) bcc solid solution	
		t (h)	t_{eq} (h)	t (h)	t_{eq} (h)	t (h)	t_{eq} (h)
150	1	up to 50		20 to >150		>150	
250	4.6	up to 10	46	10-20	46-92	50	230
350	12.7	up to 2	25.4	5	63.5	10	127

Intermetallics. Vol. 16. Núm. 3. 2008. Pag. 470-478
http://dx.doi.org/10.1016/j.intermet.2007.12.011

Table 2

Milling time ranges for the three types of MS fittings performed: a) single site at HF=33 T, b) site at 33 T plus two magnetic hyperfine field distributions and c) using a single magnetic hyperfine field distribution.

Ω (rpm)	$[\Omega/\Omega_0]^3$	a) single HF=33 T		b) HF=33 T +HF distribution		c) single HF distribution	
		t (h)	t_{eq} (h)	t (h)	t_{eq} (h)	t (h)	t_{eq} (h)
150	1	up to 10		20 to 150		>150	
250	4.6	up to 1	4.6	5-20	23-92	50	230
350	12.7	none		2-5	25.4-63.5	10	127

Intermetallics. Vol. 16. Núm. 3. 2008. Pag. 470-478
http://dx.doi.org/10.1016/j.intermet.2007.12.011

Figure captions

Figure 1. Scheme of the three reference systems used.

Figure 2. Detachment distance between ball and vial wall during flight for 150, 250 and 350 rpm, the crosses show the moment of collision. The inset shows the linear relationship between the time of flight, t_f, and the rotational period of the main disk, T.

Figure 3. Left; inertial reference system: solid line, ball trajectory, dashed line, trajectory of the centre of mass of the vial, dotted circles show the vial position at the detachment and collision events. Right, non-inertial system: Circle represents the vial; thick line, ball trajectory; straight solid lines indicate the detachment point of the ball from the wall at the detachment time, P_D, and at the collision time, P_D'; P_C indicates the collision point of the ball; δ is the angle between P_D' and P_C.

Figure 4. Normal force exerted over the ball (continuous line) and analytical solution of equation 6 (dotted line) during one period of the main disk rotation calculated for Ω=150 rpm.

Figure 5. DSC scans of $Fe_{75}Ge_{20}Nb_5$ samples after 150 h milling at different frequencies.

Figure 6. a) Powder particle size as a function of actual time and equivalent time. b) Average Cr content as a function of actual time and equivalent time.

Figure 7. XRD patterns of samples after different milling times at different milling intensities. Crosses, bcc-Fe; square, fcc-Ge; circles, bcc-Nb; triangle, intermetallic.

Figure 8. a) Angular position, 2θ, and b) full width at half maximum, FWHM, of the (110) diffraction maximum of the α-Fe(Ge,Nb) phase as a function of actual time (above) and equivalent time (below). c) Area fraction of fcc Ge and bcc Fe phases

Figure 9. Mössbauer spectra of samples after different milling times at different frequencies.

Intermetallics. Vol. 16. Núm. 3. 2008. Pag. 470-478
http://dx.doi.org/10.1016/j.intermet.2007.12.011

Figure 10. a)Average hyperfine magnetic field, <HF>, and b) saturation magnetization of the different studied samples as a function of actual time (above) and equivalent time (below).

Intermetallics. Vol. 16. Núm. 3. 2008. Pag. 470-478
http://dx.doi.org/10.1016/j.intermet.2007.12.011

Figure 1

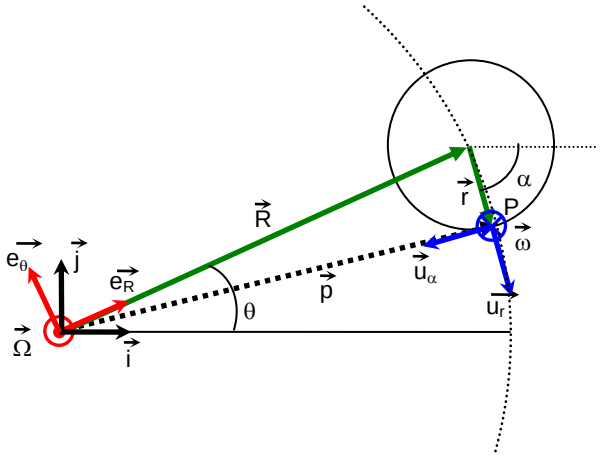

Intermetallics. Vol. 16. Núm. 3. 2008. Pag. 470-478
http://dx.doi.org/10.1016/j.intermet.2007.12.011

Figure 2

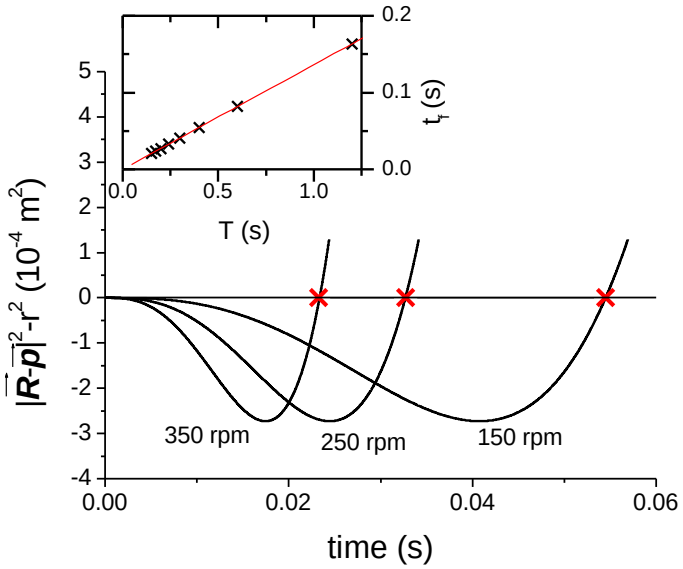

Intermetallics. Vol. 16. Núm. 3. 2008. Pag. 470-478
http://dx.doi.org/10.1016/j.intermet.2007.12.011

Figure 3.

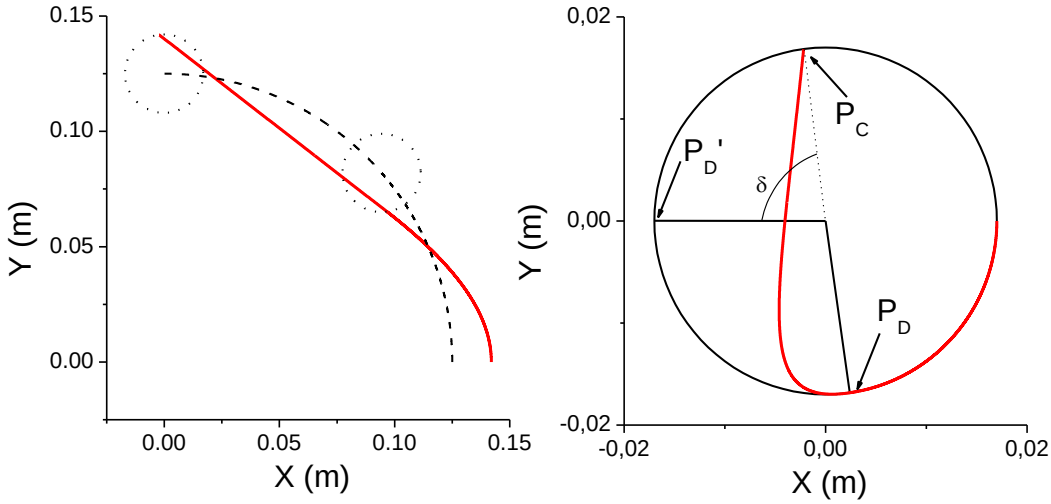

Intermetallics. Vol. 16. Núm. 3. 2008. Pag. 470-478
http://dx.doi.org/10.1016/j.intermet.2007.12.011

Figure 4.

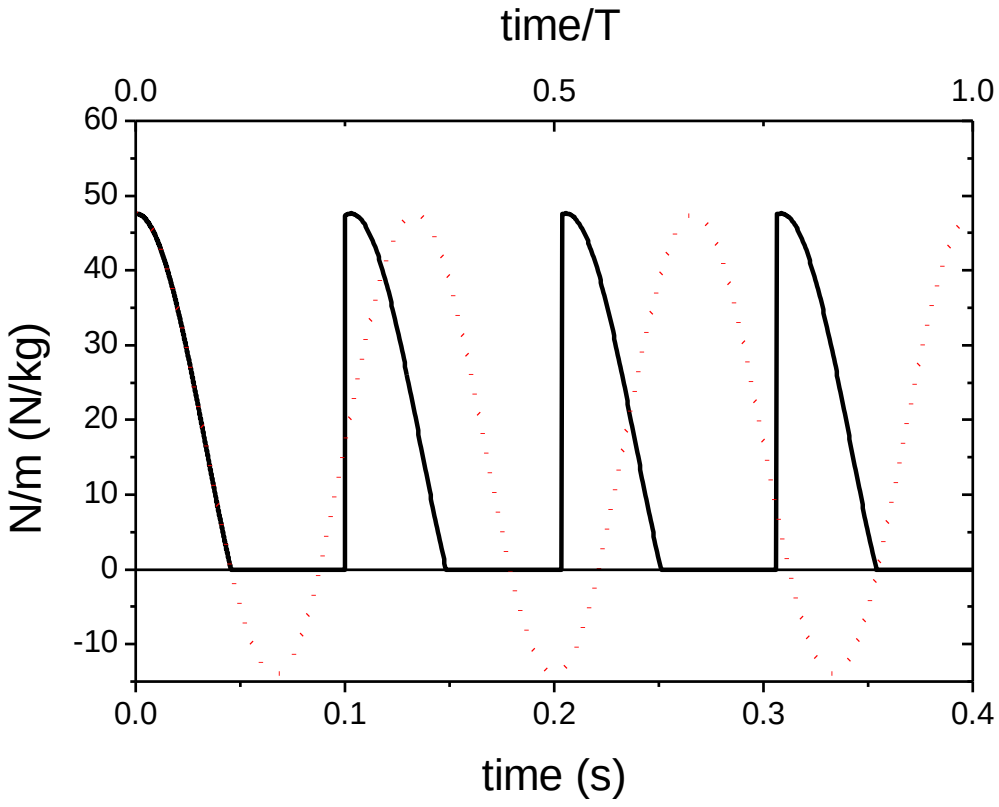

Intermetallics. Vol. 16. Núm. 3. 2008. Pag. 470-478
http://dx.doi.org/10.1016/j.intermet.2007.12.011

Figure 5.

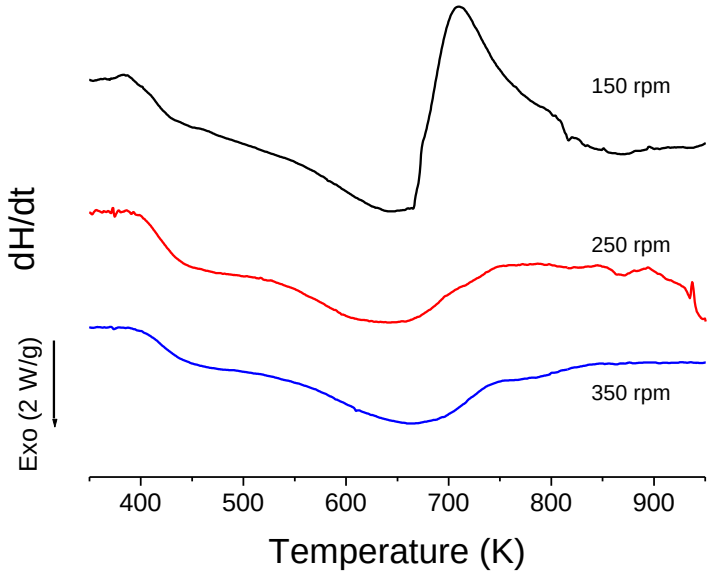

Intermetallics. Vol. 16. Núm. 3. 2008. Pag. 470-478
http://dx.doi.org/10.1016/j.intermet.2007.12.011

Figure 6.

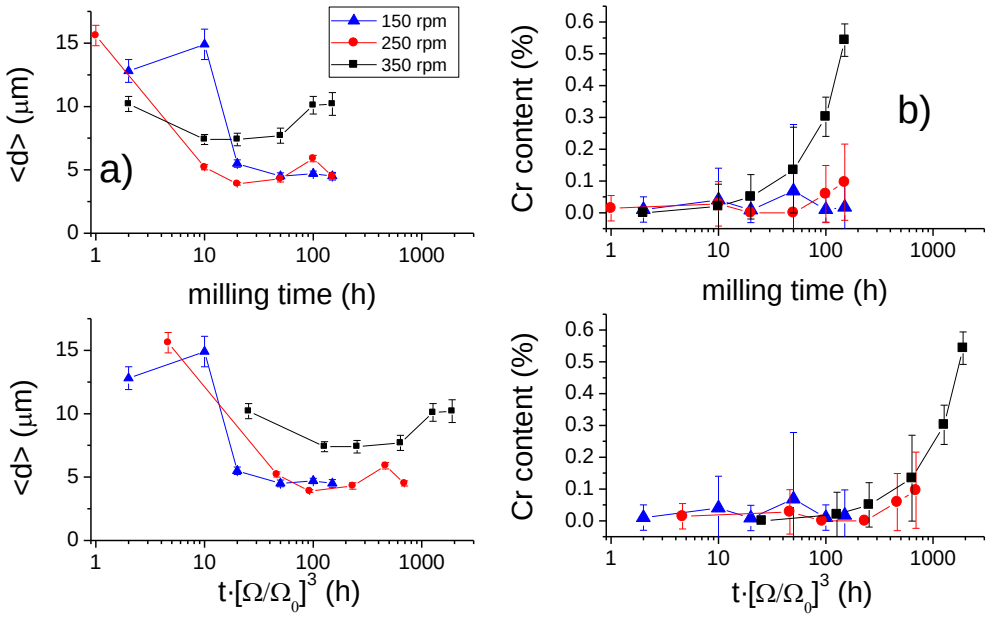

Intermetallics. Vol. 16. Núm. 3. 2008. Pag. 470-478
http://dx.doi.org/10.1016/j.intermet.2007.12.011

Figure 7.

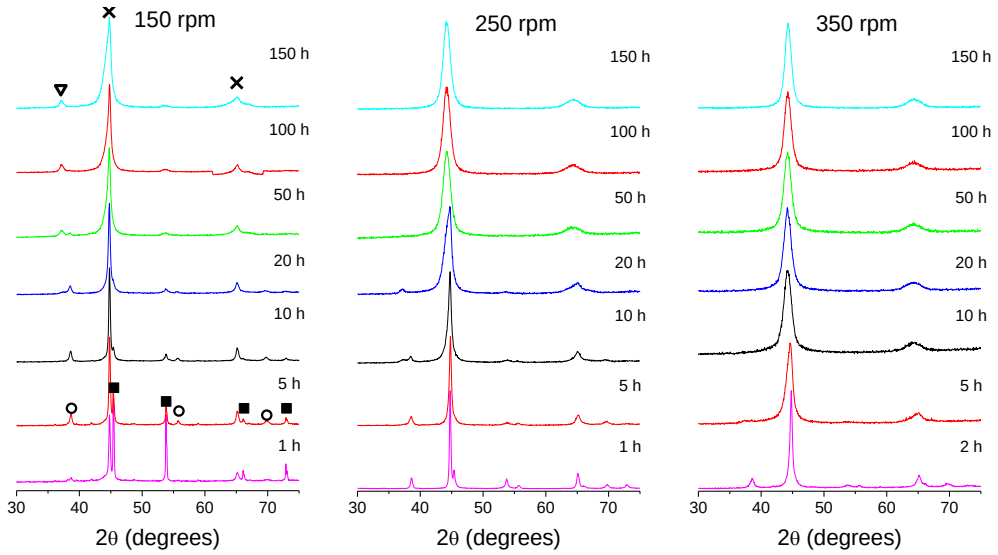

Intermetallics. Vol. 16. Núm. 3. 2008. Pag. 470-478
http://dx.doi.org/10.1016/j.intermet.2007.12.011

Figure 8.

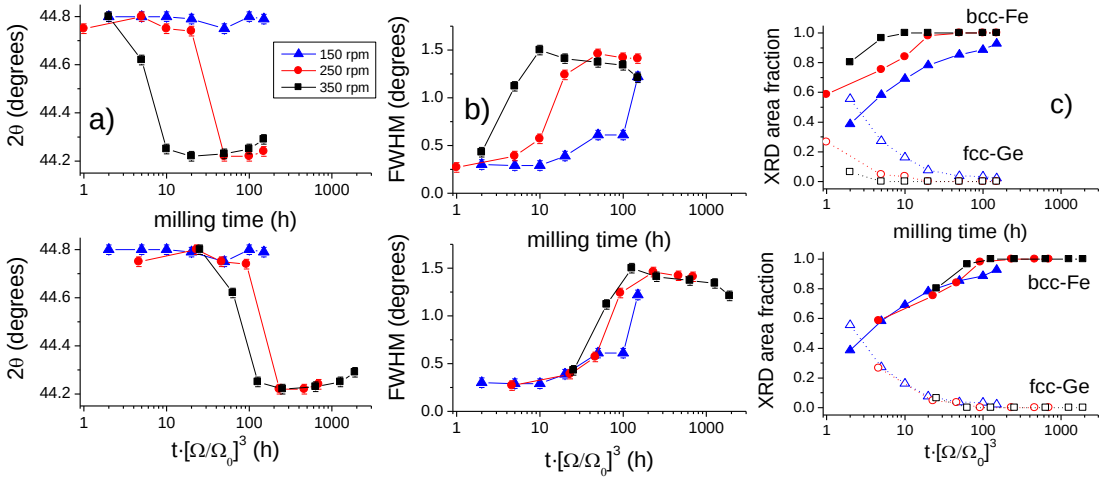

Intermetallics. Vol. 16. Núm. 3. 2008. Pag. 470-478
http://dx.doi.org/10.1016/j.intermet.2007.12.011

Figure 9.

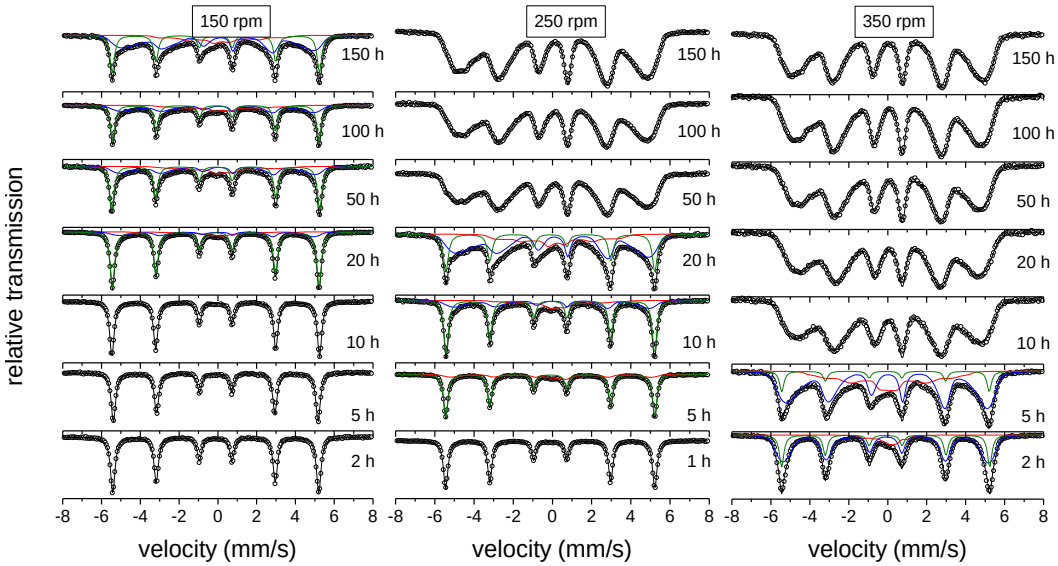

Intermetallics. Vol. 16. Núm. 3. 2008. Pag. 470-478
http://dx.doi.org/10.1016/j.intermet.2007.12.011

Figure 10.